Settlement Rate Increase in Organic Soils Following Cyclic Loading

Lemnitzer, A.[1], Yniesta, S.[2], Cappa, R.[3] and Brandenberg, S.J.[4]*

Abstract:

Post-shaking settlements observed during centrifuge tests of model levees resting atop soft compressible peat are compared with numerical settlement solutions. Two large scale (9m) tests and one small scale (1m) test are analyzed. The models included extensive instrumentation consisting of pore pressure sensors, accelerometers, bender elements, and displacement transducers to measure levee response during and following the application of scaled ground motions at the container base. Post cyclic settlement records suggested an increase in settlement rates within peat upon cyclic loading compared to pre-seismic settlements due to the combined effects of excess pore pressure generation and secondary compression. The observed settlements were compared with the predictions of a one-dimensional nonlinear consolidation code that follows an implicit finite difference formulation. The code includes nonlinear compressibility and permeability properties, and models secondary compression strain rate as a function of soil state rather than as a function of time. Secondary compression was found to be the largest contributor to levee settlement. Further, cyclic straining was found to increase the secondary compression rate after earthquake shaking. Incorporating secondary compression reset into settlement predictions resulted in close agreement with measurements, while failing to consider secondary compression reset resulted in substantial under-prediction of experimental settlement records.

Keywords: secondary compression, settlements, embankment, levee, organic soil, peat

[1] Associate Professor, Department of Civil & Environmental Engineering, University of CA Irvine, Irvine, CA, USA
[2]* Assistant Professor, Department of Civil, Geological and Mining Engineering, Polytechnique Montréal, Montréal, *corresponding author: samuel.yniesta@polymtl.ca*
[3] Project Engineer, Simpson, Gumpertz & Heger Consulting Engineers, Irvine, CA, USA
[4] Professor and Associate Dean, Department of Civil & Environmental Engineering, University of CA Los Angeles, Los Angeles, CA, USA

Introduction and Literature Review

Organic soils are among the softest, most compressible geomaterials and construction of infrastructure on peat is often avoided due to poor foundation conditions. However, constructing infrastructure on peat cannot always be avoided. For example, approximately 1800 km of levee in the Sacramento / San Joaquin Delta prevent low-lying "islands" from flooding, and many of these levees rest atop peat (Deverel et al., 2016). Accurately predicting the settlement of these highly compressible materials due to primary consolidation and secondary compression is therefore important. Furthermore, peat deposits often exist in seismically active regions, and seismic loading may accelerate settlement of peat due to primary consolidation following development of shaking-induced excess pore pressures and increase in the rate of secondary compression.

Compressibility

Following Karl Terzaghi's introduction of a 1D compression analysis in 1923 (Terzaghi, 1923), a large amount of research has shaped our understanding of the complex settlement behavior of peat via laboratory, field, and centrifuge studies. Early laboratory investigations studied the consolidation behavior of peat via oedometer and triaxial testing and provided insight into the influence of the micro and macro fiber structure in the peat, drainage paths, and volume change behavior (e.g., Adams 1963, Wilson and Lo, 1965, MacFarlane and Radforth 1965). Continued research built upon this early experimental knowledge and proposed analytical frameworks for estimating consolidation settlements considering various parameters such as creep rate, water content (w), organic content (OC), compression index (C_C), coefficient of permeability (k), elastic modulus (E), load increment ratio, and vertical effective stress (σ_v') (e.g., Berry and Poskitt 1972, Lefebvre *et al*. 1984, Kogure *et al*. 1986, Den Haan 1996, Mesri *et al*., 1997, Meyer *et al*., 2011, Lui *et al.,* 2016).

Traditionally, cohesive soils are modeled using a simple time-dependent, two-stage consolidation settlement framework consisting of (1) primary consolidation and (2) secondary compression, where the latter starts after the end of the former (Figure 1). This assumption results in a unique end-of-primary (EOP) normal consolidation line (NCL). Based on this "traditional" approach, the settlement resulting from secondary compression (S_s) is formulated as a function of time (Eq. 1), where C_α represents the coefficient of secondary compression, e_0 is the initial void ratio, H_0 is the initial thickness of the layer, t designates time, and t_p is the time at the "end of primary consolidation".

$$S_s = \frac{C_a}{1+e_0} H_0 log \frac{t}{t_p} \quad (1)$$

However, early investigations which studied the mechanisms of volumetric settlements have suggested the existence of "*secondary time effects*" in organic soils (Gray 1936). Buisman (1936) stipulated that "secular compression" (which we refer to today as "secondary compression"), occurs concurrently with direct compression in the primary consolidation phase, while it occurs exclusively in the secondary phase. Taylor and Merchant (1940) provided one of the first mathematical treatments of combined primary and secondary compression, yet, designated the primary consolidation and secondary compression to occur in a consecutive sense as treated by the traditional *e-log*$_{10}$*(t)* relationship in current literature. Potential shortcomings of this "concept of time" and the strict separation of settlement mechanisms were further recognized by Bjerrum (1967) who advocated that volumetric strain rates in soil depend on the soil state [i.e., the position in *e*-log$_{10}$(σ_v') space], rather than being a function of time. Bjerrum's Rankine lecture (1967) introduced the terms "instant" and "delayed" compression as the reaction of cohesive materials to an increase in effective stresses. This alternative interpretation proposes that secondary

compression occurs simultaneously with primary consolidation, resulting in an end-of primary (EOP) NCL that depends on the consolidation time, and therefore on layer thickness. Other models that treat secondary compression as a state-based process rather than a time-based process include Kutter and Sathialingam (1992) and Brandenberg (2017). Even though many researchers acknowledge the artificial separation of primary consolidation and secondary compression as shortcoming in traditional literature (e.g., Kutter and Sathialingam, 1992; Long and Boylan, 2013), most studies today continue to use the widespread time-dependent consolidation concept. To the authors' knowledge, only Brandenberg (2017) has proposed a direct formulation for settlements in cohesive soils that considers a time-dependent, yet simultaneous, occurrence of primary and secondary mechanisms, leaning on the early concepts recognized above. This formulation, coded into a publicly available consolidation software (iConsol.js), is used in the numerical part of this paper to compare settlement predictions with experimental records.

A common parameter used to describe the general compressibility of soil materials is the settlement index ratio C_α/C_c, which describes the ratio of secondary compression $C_\alpha$vs. primary consolidation C_c. Mesri *et al*. (1997) investigated the high secondary compression index (C_α) of various peats and found that the average ratio of C_α/C_c~ 0.06 for peats is approximately three times higher than that of granular soils. To make matters worse, C_c is often an order of magnitude higher for organic soils than for inorganic materials. Similar results were obtained by Zhang and O'Kelly (2013) who studied various effective stress theories applied to peat via consolidated-drained triaxial testing. Dhowian and Edil (1980) conducted a series of 1D consolidation tests of Wisconsin peat with a specific focus on the peats microstructure and even proposed a tertiary stage of compression associated with an increase in rate of settlement in e-$\log_{10}t$ space.

Dynamic Response

For seismic regions containing peat, the cyclic behavior of organic materials may become a major component for the determination of site response. Stokoe *et al*., 1994, Boulanger *et al*., 1998, Kramer 2000, Wehling *et al*., 2003, and Tokimatsu and Sekiguchi 2007 are among some of the more recent studies which investigated the effects of loading frequency, cyclic degradation, and stress history via laboratory testing, and proposed relationships for modulus reduction and damping (Kishida *et al*., 2009). Egawa *et al*. (2004) investigated the behavior of embankment structures on soft peat via centrifuge experiments, with a specific focus on the effects of model geometry and input motions on the accelerations and strains developed in the foundation soil, however; Egawa *et al.* did not describe the volumetric changes and pore pressures generated in the peat itself. Shafiee *et al.* (2015) and Shafiee (2016) studied the settlement rates of cyclically loaded Sherman Island peat via direct simple shear and triaxial testing and discovered that the peat generates excess pore pressure during cyclic loading when shear strains exceed about 1%. Perhaps more importantly, Shafiee *et al*. found that cyclic loading may increase the secondary compression settlement rate, which in turn has the potential to accelerate settlements of embankment structures that just survived strong shaking, and are then faced with potential internal instability; which may lead to their failure (by reducing levee freeboards and triggering levee overflow/breach). Shafiee *et al.* (2015) and Shafiee's (2016) study furthermore observed that the secondary compression rate increased when cyclic shear strains and the number of cycles increased. Specifically, secondary rate increase was noted when shear strains exceeded a threshold of about 0.1% for low OC peat and 0.7% for high OC peat. Cappa *et al.* (2017) investigated the development of strains and pore pressures during centrifuge testing of model levees resting on peat and subject to various ground motions. Shear strains as high as 7% were mobilized in the peat for ground motions with peak base

accelerations of 0.53g. Cappa *et al.* observed the shear strain threshold beyond which excess pore pressures are generated in the peat to be near 1.0%. This strain level is consistent with the direct simple shear laboratory studies for peat with similarly high organic content, e.g. 0.7% and above as shown in Shafiee *et al.* 2015. The maximum residual excess pore pressure ratio recorded during Cappa *et al.*'s centrifuge tests was 0.2. Comparable shear strain ranges and excess pore pressure ratios for peats from the Delta region tested in triaxial studies were also observed by Wehling *et al.* (2003). These residual excess pore pressures are potentially important due to the post-earthquake settlements that arise from reconsolidation. Although the residual excess pore pressure ratios are modest, the compressibility of the peat is very high, and post-cyclic volumetric strains are potentially significant.

To better understand the influence of cyclic loading and seismically induced excess pore water pressure on the settlement rates of organic soils, data from centrifuge tests of three stiff embankment structures on soft peat are analyzed. The primary objective of this study is to compare measured post-earthquake settlement rates with predictions. This objective is achieved by: (1) quantifying earthquake-induced strains in the peat layer using embedded accelerometers, (2) relating the observed cyclic strains to pore pressure increase and secondary compression reset, (3) compute post-cyclic settlement using a nonlinear consolidation code, and (4) compare predicted settlements with observations. Finally, the benefits and the limitations of the numerical approach used herein are discussed.

Centrifuge Testing Program

A series of centrifuge experiments consisting of sand and clay levee structures placed atop organic foundation soil were conducted on the small (1m) and large (9m) centrifuges at the Center for

Geotechnical Modeling at UC Davis (Lemnitzer *et al.*, 2016). The three experiments selected for analysis in this paper consisted of a stiff levee structure made of modeling clay (sculpting wax) placed atop a layer of peat, which in turn rested on a drainage layer of dense, coarse sand. Figure 2 and Table 1 describe the model geometries in prototype scale associated with each experiment. A detailed description of all experimental work, including data reports and recommended usage of digital data, is provided in Lemnitzer *et al.*, 2016. Data from the experimental study have been curated and published, and the experiments utilized in this study are Exp. 12 (Cappa *et al.*, 2014a), Exp 14 (Cappa *et al.*, 2014b), and Exp 16 (Lemnitzer *et al*., 2020). Exp 12 and 14 were conducted on the large centrifuge (9m radius) and setup in a rigid container with dimensions of 1.76m in length, 0.91m in width and 0.54m in height. Exp 16 was spun on the small centrifuge (1m radius) and setup in a rigid container with dimensions of 0.56m in length, 0.28m in width and 0.18m in height.

Each model was instrumented with accelerometers, linear potentiometers, pore pressure transducers, and bender elements to measure the model response. For clarity, sensors are omitted from Figure 2, but are included in subsequent data analysis plots and can also be viewed in the data report for each experiment. Testing of the large-scale experiments (Exp 12) and (Exp 14)) was conducted at 57g while the small-scale experiment (Exp 16) was conducted at 50g, after over-consolidating the model at 60g, hereby generating an over-consolidation ratio (*OCR*) of approximately 1.2 in the peat. The large-scale experiments were subjected to a series of motions consisting of sine waves and scaled ground motions (i.e., scaled Kobe & Loma Prieta earthquakes) as listed in Table 2. Only two motions (scaled Maule, 2010, and a sine-sweep) were applied to the 1m centrifuge test (Exp 16). The frequency range of the sine waves spanned from 0.12 Hz to 5.8

Hz, had constant velocity amplitudes and lasted an average duration of 3 seconds in prototype scale.

Properties of the soil materials utilized for the centrifuge experiments are shown in Table 3 for peat, dense sand, and modeling clay. The peat was excavated from a depth of 2-3 m at Sherman Island in the Delta and transported in sealed plastic lined steel drums to the centrifuge facility at UC Davis. The peat had an organic content of 69%, the inorganic component being gray clay. During storage and handling, the peat remained submerged to avoid desiccation. The peat contained long fibers and clusters that were removed to obtain a more homogeneous material suitable for the centrifuge model. The peat was placed as a slurry on top of the coarse dense sand layer, and lightly consolidated beneath a thin layer of sand that was removed prior to installing the clayey levee. The dense layer of coarse sand (Figure 2) was placed via dry pluviation at the bottom of the container. The coarse sand material had a unit weight of 20.2 kN/m^3 and an approximate relative density D_R of 90%. This layer was added to simulate a common stratigraphy encountered in the Delta and to provide a drainage stratum for the peat during consolidation. The clayey levee was constructed using oil-based sculpting/modeling clay with a unit weight of 18 kN/m^3. Shear wave velocity of the modeling clay measured at 1 g was about 400m⁄s. Shear wave velocities of the different materials were measured via bender elements placed in the respective layers. Shear wave velocity parameters V_{s1} and n were obtained through data fitting as explained in detail in Cappa *et al.*, 2012 and are listed in Table 3 for peat and sand, respectively.

Data Analysis

Experimental settlements in free field and center levee arrays: Time histories of Slow Data

Figure 3 presents the g-field, pore pressures and settlement time histories for all experiments recorded at a data sampling rate of 1 Hz in model scale (left axis) and prototype scale (right axis). These data are referred to as "slow data", since their sampling rate is much slower (compared to sampling rates during earthquake loading) and equates to "long term monitoring" in in-situ configurations. Following spin-up, each model was allowed to consolidate until excess pore pressures were essentially zero prior to applying the ground motions listed in Table 2 and shown as dashed lines in Figure 3. For Exp 12, during spin up and primary consolidation at 57g, the peat in the center levee array settled approximately 7.3 cm / 4.16 m in model / prototype scale respectively. This settlement is attributed to the peat and corresponds to 40% vertical strain for this test. The free field peat in Exp 12 settled about 3.5 cm / 2.0 m in model / prototype scale respectively, which corresponds to 21% vertical strain, respectively. Similar strain magnitudes were observed for Experiments Exp 14 and Exp 16. Prior to testing on the large centrifuge, the amount of settlement during spin-up was estimated via small-scale testing of simplified levee structures in the 1m centrifuge. The targeted and achieved peat thickness after spin-up and at the end-of primary consolidation was representative of common prototype peat layers of about 3-12 m found in the Delta (Atwater and Belknap, 1980). Figure 3 includes time histories for the center levee array and the free field for Exp 12 and Exp 14. Free field measurements for Exp 16 are omitted in Figure 3 because the free field linear potentiometer failed during testing.

Co-Seismic and Post-Seismic Settlement Records

Earthquake-induced levee settlement can be divided into co-seismic and post-seismic components. The co-seismic settlement occurs so quickly that it is not visible in the "slow data" records (as presented in Figure 3), but can be observed using "fast data", which are records sampled at a frequency of 4096 Hz and used to capture the dynamic response of the model during application

of the ground motions. Post-seismic settlements start at the end of shaking and continue until application of the next ground motion in the sequence. In general, the next ground motion was only applied when seismically induced pore pressures reached pre-earthquake values. Settlement during this time period is due to a combination of primary consolidation and secondary compression and waiting longer between shaking events will therefore result in more settlement due to secondary compression.

Example fast data records are shown in Figure 4 for the large Kobe motion for Exp 14 and the Maule, Chile motion for Exp 16. Figure 4 presents base acceleration, pore pressure at the center of the peat beneath the levee crest, and settlement of the levee crest. The low frequency portion of the settlement record was obtained using a vertical linear potentiometer mounted to the levee crest, while the high frequency portion was obtained by double-integrating the vertical accelerometer record at the top of the levee crest. A high-pass filter was applied to data recorded with accelerometers, while a complementary low-pass filter (i.e., the low-pass and high pass filters add to unity at all frequencies) was applied to the linear potentiometer data and the two filtered records were added to obtain the settlement shown in Figure 4.

As shown in Figure 4a, the Large Kobe motion applied to Exp 14 generated excess pore pressures of about 6.9 kPa in the peat beneath the center of the levee. In the free field array (not depicted in the graph), the pore pressure increased by only 1.1 kPa. This is expected given the much higher effective vertical stress beneath the levee (approx. 50 kPa) compared to the low effective overburden pressure (3kPa) in the free field. The total prototype settlements recorded during and after the Large Kobe motion yielded measurements of approximately 26 cm and 23 cm beneath the levee crest and in the free field, respectively. The settlement is divided among the following components: co-seismic settlements of approximately 6.5 cm and 2.9 cm, and post-

seismic settlements (i.e., primary consolidation and secondary compression) of 19.3 and 20.0 cm underneath the levee and free field respectively.

Figure 4 also depicts the pore pressure development and settlements of the 1m centrifuge experiment (Exp 16, Figure 4b) at the center of the model (i.e., underneath the levee structure). The Maule, Chile motion generated an increase of pore pressures Δu, of 3.2 kPa underneath the center of the levee. Settlements were recorded using LVDT L4, which was placed atop the levee structure, similar to Exp. 14. A co-seismic settlement of 5.0 cm was recorded underneath the levee center.

Rate Increase following Seismic Loading

The large Kobe motion applied to Exp 14 as well as the Maule, Chile motion applied to Exp 16 were selected to demonstrate the change in settlement rates before and after cyclic loading. Figure 5 depicts an enlarged detail of pore pressure and settlement records taken from the slow data records of Exp 16. As earthquake loading is applied, the pore pressures experience the sudden jump depicted in Figures 3c and 4b, followed by pore pressure dissipation to nearly pre-earthquake levels. Simultaneously, a sudden increase in settlements (co-seismic) is observed during loading followed by a slow, steady, accumulation of post-seismic settlements. As stipulated in the introduction, these settlements result from simultaneously occurring primary consolidation and secondary compression. Pre- and post-loading settlement rates, $\dot{s}_0$ and $\dot{s}_1$, respectively, obtained by approximating the slope of settlement data as shown in Figure 5, are compared at similar pore pressure levels following the seismic loading. While the increase in settlement rates might not be obvious in the linear time scale used for Figure 5, analyses of pre- and post-settlement rates showed a clear increase. For instance, for Exp 16, the pre-and post-earthquake (after dissipation of excess

pore water pressure) rates were $\dot{s}_0$ = 16.6cm/day and $\dot{s}_1$ = 21.5 cm/day respectively, which corresponds to a 30% increase in settlement rate following seismic loading.

Determination of shear strains for subsequent settlement analyses

A detailed description of the derivation of cyclic shear strains from centrifuge data is published in Cappa *et al.* (2017). Cyclic shear strains must be known in order to compute the values of the secondary compression reset index I_r as well as the residual excess pore pressure ratios $r_{u,r}$, as explained in the numerical modeling section of this paper. The residual excess pore pressure ratio $r_{u,r}$, is determined by dividing the excess pore pressures at the end of the seismic motion by the effective vertical overburden pressure at the location of the pressure sensor. Shear strains were determined from accelerometer readings recorded in the peat underneath the levee. The strain path in the peat beneath the levee is more complicated than that used in Shafiee's direct simple shear laboratory test program (Shafiee *et al.*, 2015). To account for the more complex strain history in the centrifuge experiment, components of the Cauchy strain tensor $\varepsilon_{xx}, \varepsilon_{zz}, \gamma_{xz}$ are computed first from measured dynamic displacements (obtained by double integration of high-pass filtered acceleration records), and subsequently used to compute an equivalent direct simple shear deviatoric strain invariant, $\gamma_{DSS,eq}$ defined in Eq. 2. Note that high-pass filtering removes the low frequency content from the displacement records, therefore the computed strains correspond to the dynamic component. Figure 6 shows the resulting direct simple shear strain history during the application of the Large Kobe motion in Exp 14.

$$\gamma_{DSS,eq} = \sqrt{\frac{2}{3}} \cdot \sqrt{\left(\varepsilon_{xx}\right)^2 + \left(-\varepsilon_{zz}\right)^2 + \left(\varepsilon_{zz} - \varepsilon_{xx}\right)^2 + 6 \cdot \left(\frac{\gamma_{xz}}{2}\right)^2} \qquad (2)$$

The residual excess pore pressure ratio, r_{ur} can be calculated for each earthquake based on Eq (3) from Shafiee (2016), which was derived for Sherman Island peat with organic contents ranging between 10 and 70, and overconsolidation ratios (OCR) between 1.1 and 4.9.

$$r_{u,r} = 0.316(\gamma_c - \gamma_{tp})^{0.619} \cdot N^{0.187} \cdot OCR^{-0.477} \cdot OC^{-0.499} \quad (3)$$

where γ_{tp} is pore pressure generation threshold shear strain.

In order to use the Equation for $r_{u,r}$ (Eq. 3) and the reset index I_R (as introduced later in Eq. 4) an equivalent number of uniform cycles (N) and corresponding shear strain amplitude γ_c must be computed from the irregular $\gamma_{DSS,eq}$ time series shown above. This is accomplished by counting strain cycles, and weighting them in proportion to the strain amplitude, in a manner that is similar to procedures commonly utilized in liquefaction triggering analyses (e.g., Seed and Idriss, 1970). Using this method, a broadband time series is represented by a reference value of the quantity being computed (*CSR* for liquefaction triggering evaluation procedures, γ_c for the application here) at an equivalent number of uniform cycles. In this case, we solved for the value of γ_c corresponding to 15 equivalent uniform cycles. With the application of each motion, seismically induced excess pore water pressures are generated and a residual excess pore pressure ratio, r_{ur} can be calculated for each earthquake based on Eq (3).

Numerical Analyses

In 2017, Brandenberg (2017) adapted Kutter and Sathialingam's concept and formulated an alternative 1D nonlinear implicit finite difference code in which he introduced a 'reference secondary compression line' (RSCL). The secondary compression strain rate is inversely proportional to the distance between the state of the soil in e-log σ'_v space and the RSCL. Modeling

296 secondary compression in this manner enables both mechanisms to occur simultaneously. The
297 code is publicly available as a JavaScript Web-based application called "iConsol.js" at:
298 www.uclageo.com/Consolidation/. It is fully nonlinear and considers changes in permeability and
299 compressibility as settlement increases and void ratio decreases. This code is used hereafter to
300 model the centrifuge tests and simulate the rate of settlement following an earthquake.

301 The consolidation of the levee is a two-dimensional plane-strain problem. However, since
302 ratios of peat thickness to levee base width were approximately 0.3, 0.2, and 0.25 for Exp 12, 13,
303 and 14, respectively, Terzaghi et al. (1996) indicated that these ratios result in a consolidation
304 condition that can be reasonably approximated as one-dimensional. Therefore, even though the
305 iConsol.js code is one-dimensional, it can adequately model the problem.

306 Based on the proposed approach by Kutter and Sathialingam, the rate of secondary
307 compression following an earthquake would be lower than the secondary compression rate before
308 the earthquake, since seismically induced volumetric strains would reduce the void ratio, and
309 therefore increase the distance of the consolidation curve to the RSCL. However, this approach
310 contradicts the observations from cyclic simple shear tests on peat conducted by Shafiee et al.
311 2015, whose results suggest a clear increase of secondary compression settlement rates after cyclic
312 loading. Shafiee (2016) proposed an approach for modeling the change of settlement rate by
313 shifting the RSCL downward from its initial position, and towards the current point in stress-space,
314 effectively reducing the distance between the current stress point and the RSCL, hereby increasing
315 the rate of secondary compression. Assuming the RSCL is initially coincident with the normal
316 consolidation line, shifting the RSCL all the way down to the current stress point would constitute
317 a full reset of secondary compression behavior, resulting in the strain rate being identical to that
318 for a normally consolidated soil. The amount by which the RSCL is shifted from the NCL to the

current state in $e - \log \sigma_v'$ space is defined as secondary compression reset index, I_R. $I_R = 0$ corresponds to no secondary compression reset, and $I_R = 1$ means full reset. Shafiee (2016) presents an equation (see Eq. 4) for I_R as function of cyclic strain amplitude, γ_c, number of cycles, N, overconsolidation ratio, OCR, organic content, OC, and static shear stress ratio, $\alpha = \tau_s/\sigma_{vo}'$.

$$I_R = {\gamma_c}^{0.219} N^{0.261} (0.899\alpha + 0.939) \times (-0.043OC + 0.300) \left(0.192 \frac{\sigma_{vo}'}{p_a}\right) \times (0.009OCR + 0.980) \quad (4)$$

Figure 7 a,b,c schematically explains the above-mentioned principle by illustrating the settlement and pore pressure generation during a typical centrifuge experiment. The response of a compressible peat layer is described in terms of consolidation behavior (a), vertical settlement (b), and pore pressure (c). As the centrifuge is spun up, pore pressure develops in the peat and reaches a peak (point A). Note that this point, being situated away from the NCL, represents an overconsolidated state of stress. At this point settlement is caused by both, excess pore pressure dissipation and secondary compression. Once all excess pore pressure is dissipated (point B) the settlement is solely controlled by secondary compression under constant effective stress. The rate of secondary compression is inversely proportional to the distance between the current state in e-log(σ'_c) space (point B) and its projection (point B*) on the reference secondary compression line (RSCL). As secondary compression progresses, the distance between the current state and its projection increases, effectively slowing down secondary compression. At point C, an earthquake is applied, inducing significant shear strains and associated pore pressures, consequently decreasing the effective stress (to point C'). As pore pressure dissipates following the earthquake, settlement ensues until complete pore pressure dissipation (point D). However, following an earthquake, the secondary compression mechanism is now partially or completely reset, meaning

342 that the rate of secondary compression increases compared to pre-event rate. This is modeled by a
343 change in position of the RSCL (dashed line) which moves down according to the reset index (IR)
344 and renders the new projection point (point D^*) closer to the current state. As the distance between
345 the current state and its projection decreases the secondary compression rate increases.

346 ***Model Input Parameters***

347 Settlement simulations for the centrifuge tests are performed using the iConsol.js code by
348 Brandenberg (2017). The peat was modeled as single layer with multiple elements to account for
349 the variability of the material across the layer thickness. The simulations can be considered semi-
350 predictive, as the input parameters for compressibility, secondary compression, and permeability
351 were selected from laboratory tests on the peat reported by Shafiee et al. (2013). This data would
352 be similarly available to any researcher/practicing engineer. The peat used in the centrifuge and in
353 Shafiee et al.'s laboratory testing program were retrieved from the same location. Specifically, soil
354 properties presented in Table 3 were taken from the consolidation tests and the falling head tests
355 performed in Shafiee et al.'s (2013) study. The advanced settings of the consolidation code for the
356 secondary compression allow to control the position of the RSCL. When modeling the reset of
357 secondary compression after an earthquake, the value of the reference void ratio for secondary
358 compression, $e_{c\alpha,ref}$, is reduced based on a calculated reset index I_R based on Eq 4.
359 The initial overburden pressure was calculated based on the clayey levee's thickness, the unit
360 weight of the modeling clay, and the g-level. The height of the layer was calculated based on the
361 initial height of the layer measured before spin-up, and the LVDT measurement at the time of the
362 earthquake. Table 4 presents the modeling input parameters for the settlement simulation in
363 iconsol.

364

Model Calibration

The initial, experimental OCR is a critical parameter in the computation of vertical strains resulting from secondary compression. However, it is difficult to compute an accurate OCR since the peat is initially normally consolidated. As the centrifuge is spun up, the OCR increases quickly as a result of primary consolidation and secondary compression occurring simultaneously. A preliminary estimation based on initial and final void ratios, as well as measured settlements yielded inaccurate values of OCR. This inaccuracy can be attributed to the uncertainty of the NCL's position, its shape at low confinement pressure, and the important rebound of the peat. Hence, the approach pursued hereafter back-calculates the OCR at the start of each test by using the rate of secondary compression prior to the application of any ground motion as reference.

Figure 8 presents the predicted and measured settlement in the centrifuge test RCK01 during spin-up. As the centrifugal acceleration increases, the settlement increases due to the increased stresses imposed on the soil layer. Once the target g-level is reached (at approximately 3,700s) pore pressure starts dissipating, and primary consolidation controls the settlement process until all excess pore pressure is dissipated (at about 7,000s). From this point forward the settlement is controlled by secondary compression. In order to obtain a reasonable estimate of the secondary compression rate as shown in Figure 8 as "Predicted", the nonlinear consolidation code is run in an iterative manner until the rate of secondary compression before the first earthquake (at approximately 10,000s) matches the rate measured in the centrifuge. For RCK01 the OCR was about 1.25, while the OCR for RCK02 was 1.4. These values are found to be consistent with estimations of the OCR based on crude measurements of the void ratio, while the simulated settlements were close to reality. Once the OCR at the start of the test is defined, the initial void

ratio is calculated, and the OCR is updated for each motion, based on the evolution of the void ratio as settlement increases.

Comparison of numerical simulations with experimental observations

Figure 9 depicts a comparison of recorded and predicted settlements in the center levee array following three of the motions applied during Exp 12 and Exp 14 and two motions applied to Exp 16. The three ground motions selected for analysis were scaled versions of the Loma Prieta, the Kobe and the Maule, Chile ground motions. Additionally, sine sweep motions were applied in Experiment 14 and 16. For each loading scenario, three different post-earthquake settlement simulations were performed: (1) settlements resulting from primary consolidation only (i.e., C_α = 0), (2) settlements resulting from primary consolidation and secondary compression but without reset applied (i.e., $I_R = 0$), and (3) settlements resulting from primary consolidation and secondary compression accounting for reset induced by the deviatoric strain history mobilized during the various motions (as explained earlier).

The analyses become progressively more accurate as C_α and I_R are introduced. The comparison between experimental records and numerical analyses shows that secondary compression is the primary source of settlement, with primary consolidation contributing a relatively small fraction, except for the larger motions. It is evident that settlements are under-predicted when secondary compression reset is ignored. Only the inclusion of the reset mechanism (i.e., the integration of the accelerated secondary compression rate after seismic loading) can capture the measured settlements and yield an accurate prediction of the results. While both analysis options without the compression reset substantially underpredict the experimental

settlements, accounting for the reset approximates the experimentally recorded values within an accuracy of about 15%.

Discussion

Analytical Results

Figure 10a presents the measured and predicted settlement records versus peak base acceleration. Settlement records and predictions are evaluated at the end of the settlement histories depicted in Figure 9. These time frames assume that secondary compression was well underway, and that post-earthquake pore pressures reached pre-shaking pore pressure magnitudes. Similar to Figure 9, it is evident that the omission of the secondary compression reset yields substantial underpredictions of the observed settlement measurements, with errors of up to 100% (e.g., sine sweep, EXP 14). The smallest error for any settlement simulation that includes secondary compression but ignores the reset mechanism was found to be 53% (Exp 16, Maule, Chile EQ). The median error for settlement predictions without secondary compression reset was 84% and for settlement predictions that only considered primary consolidation 89%. However, the median error between settlement predictions with secondary compression reset and experimental observations was only 15%.

Figure 10b evaluates the predictive accuracy of all displacement analyses types using a residual analysis. All ground motions applied to the centrifuge models per Lemnitzer *et al.*, 2016 are included in this graph (i.e., including those not presented in Figure 3). Displacement residuals were determined in log space as $R = \ln(s_{measured}) - \ln(s_{predicted})$. Figure 10b suggests that only the inclusion of a secondary compression reset yield results with minimal residual displacements. Among the predictions accounting for the secondary compression reset, a slight underestimation of settlements for small Peak Base Accelerations (PBA's) and increase of prediction accuracy with

increasing PBA's is observed. The largest residual was calculated to be 0.5 while the smallest residual was 0.07.

Benefits and Limitations of the Numerical Approach

The proposed analyses including secondary compression reset provide considerably better settlement estimates as indicated by the preceding error analysis. However, benefits and limitations inherent to the analyses and the selection of input parameters are discussed hereafter to provide perspective.

The authors worked with highly characterized materials and conducted extensive laboratory testing to obtain the material parameters under different test conditions. In order to keep the above-presented simulations semi-predictive, the laboratory input parameters (and not the centrifuge specific properties) have been selected as input for the iConsol.js analysis as explained above. Using laboratory-based input parameters vs. in-situ (aka centrifuge-based parameters) enabled the separation of potential errors within the settlement estimates, inherent to the model input compared to truly predictive analyses.

The laboratory-based parameters can be obtained in similar fashion by other engineers. Specifically, the difficulties in properly defining OCR of the peat pertains to centrifuge testing only, and does not apply to field conditions. In our centrifuge experiment, the peat was sieved to remove coarse fibers and positioned in the container by scooping. The peat was then consolidated under its own-weight upon spin-up. As a result, it is not possible to retrieve an undisturbed sample of the peat and perform consolidation testing. On the contrary, retrieving relatively undisturbed specimens of peat in the field is straightforward, and performing consolidation testing suffices to define all compressibility parameters accurately, including the OCR. Hence practicing engineers

456 could much more easily obtain the necessary consolidation input parameters compared to our
457 centrifuge model.

458 Secondary compression properties can also be defined from consolidation test results by
459 setting the initial RSCL as the NCL associated with the time necessary to reach the end of primary
460 consolidation. The permeability properties can be computed via falling head tests or taken from
461 published literature. Note that the evaluation of Ck requires running several falling head tests at
462 different void ratios, however, the variation of Ck has a limited impact on the analysis results
463 compared to the initial value of permeability.

464 The definition of input shear strain histories poses a limitation to the quick execution of
465 the settlement analysis. The embedded accelerometers permitted us to compute deviatoric strains
466 mobilized during shaking. Strain histories for all of our levee-soil configurations were obtained by
467 Cappa et. al (2017) for each specific centrifuge experiment. Problem specific strain histories are
468 not available for a project conducted in practice. We suggest that for major projects with adequate
469 budget for laboratory testing and dynamic analysis, engineers conduct laboratory testing to
470 characterize the pore pressure response and secondary compression reset behavior of the soils of
471 interest, and subsequently perform dynamic analysis to characterize deviatoric strain demands.
472 These inputs can then be utilized to predict post-earthquake settlements in the manner illustrated
473 in this paper.

474 Shear strains could also be estimated alternatively by taking the ratio of peak ground
475 velocity and average shear wave velocity in an approximate manner, or by performing site
476 response analysis. Unfortunately, these approaches will merely approximate strain magnitudes,
477 yet, could provide much closer overall settlement estimates compared to traditional consolidation

analyses. A simplified procedure for practice-oriented applications is currently under development by the authors, and thus outside the scope of the current study.

As mentioned above, the rate of settlement measured in the centrifuge models may differ from the rate predicted by the iConsol.js code, because the centrifuge models were three-dimensional (although the center of the model could be represented by a 2D plane strain model) whereas the simulations are one-dimensional. For instance, lateral pore pressure dissipation would not be captured by the code. However, the secondary compression phenomenon taking place beneath the levee controlling the settlement is likely to be one dimensional, although shear creep might contribute to the overall deformation pattern. In addition, the code considers one homogeneous layer of peat which might not be an accurate representation of the soil beneath the levee. For instance the stress distribution might induce an overconsolidation ratio not constant with depth. However, because the width of the levee is greater than the peat thickness, the differences are likely to be small, and the 1D assumption appears reasonable, which is supported by the good match between the simulations and the observations.

Summary

Accurately predicting the settlement of highly compressible soils, such as peat, due to primary consolidation and secondary compression is particularily important in seismically active regions, where earthquake loading may accelerate the settlement of peat due to shaking-induced excess pore pressures and increase in rate of secondary compression. Three centrifuge experiments provided experimental settlement records of non-liquefiable levee structures resting on peat. The levee structures were subjected to various ground motions with peak base accelerations ranging from 0.02g to 0.95g in prototype scale. The response behavior of the levee-soil system was recorded through internal and external sensors, such as LVDTs, pore pressure sensors,

accelerometers, and bender elements. Post-cyclic setttlements in the peat were analyzed using sensor instrumentation and compared with one-dimensional numerical analyses using the software iConsol (available at www.uclageo.com/Consolidation). The iConsol.js software package either includes or disregards secondary compression and the reset of secondary compression due to cyclic loading. The secondary compression reset mechanism accounts for the change of settlement rate following a seismic event by shifting the reference secondary compression line downward from its initial position, and towards the current point in stress-space, hereby effectively reducing the distance between the current stress point and the reference secondary compression line, and inherently increasing the rate of secondary compression. The settlement analysis furthermore accounts for a simultaneous occurance of primary consolidation and secondary compression throughout the entire settlement process.

A comparison of experimental settlements with traditional predictions considering primary consolidation only, yielded a median error of 89 % between observed and recorded measurements. Analyses that included secondary compression but ignore its reset under-predicted the observed settlements with a median error of 84%.

Only the accurate consideration of simultaneously occuring primary consolidation and secondary compression and the inclusion of the secondary reset mechanism provided close estimations of experimental settlements. A median error of only 15% between measurements and predictions validates that the two settlement mechanisms occur simultaneously with reset, while under-predictions may arise from the "traditional" method for computing secondary compression settlement.

Data Availability Statement

All data used during this study are publicly available in the DesignSafe CS online repository in accordance with funder data retention policies.

Acknowledgements

This research was funded by the National Science Foundation under grant No. CMMI 1208170. Any opinions, findings, and conclusions or recommendations expressed in this material are those of the author(s) and do not necessarily reflect the views of the National Science Foundation.The writers would like to acknowledge the valuable assistance of the UC Davis centrifuge team.

References

Adams,J.I. l963 “A Comparison of Field and Laboratory Consolidation Measurements in Peat.” *Proc. of 9th Huskeg Research Conf.*, NRCC, 117-135.

Atwater BF, Belknap DF 1980 “Tidal-Wetland Deposits of the Sacramento-San Joaquin Delta”, In *Quaternary depositional environments of the Pacific coast: Pacific coast paleogeography symposium 4*. (eds Field ME, Bouma AH, Colburn IP, Douglas RG, Ingle JC), pp.89–103. The Pacific Section of the Society of Economic Paleontologists and Mineralogists, Los Angeles, California

Berry, P. L. and Poskitt, T. J., "The Consolidation of Peat," *Geotechnique,* Vol. 22, No. 1, March 1972, pp. 27-52.

Bjerrum, L. 1967. “Engineering geology of Norwegian normally consolidated marine clays as related to settlements of buildings.” *Geotechnique*, **17**(2), 83–118.

Brandenberg, S.J. 2017. “iConsol.js: JavaScript Implicit Finite-Difference Code for Nonlinear Consolidation and Secondary Compression.” *International Journal of Mechanics*, ASCE http://dx.doi.org/10.1061/(ASCE)GM.1943-5622.0000843

Boulanger, R.W., Arulnathan, R., Harder, L.F.J., Torres, R.A., and Driller, M.W. 1998. “Dynamic Properties of Sherman Island Peat”, *Journal of Geotechnical and Geoenviromental Engineering*, ASCE, 124(1): 12-20.

Buisman, A. S. K. 1936 , "Results of Long Duration Settlement Tests," in *Proceedings of the First International Conference on Soil Mechanics and Foundation Engineering.* Vol. 1, Harvard University, Cambridge, 1936, pp. 103-106.

555 Cappa, R., Yniesta, S., Brandenberg, S., Stewart, J., Lemnitzer, A. 2014a. "TEST 12L - RCK01
556 : Part 1 - 9m radius centrifuge experiment on clayey levee behavior under ground motions",
557 Network for Earthquake Engineering Simulation (distributor),
558 Dataset, DOI:10.4231/D34M91B6S

559 Cappa, R., Yniesta, S., Brandenberg, S., Stewart, J., Lemnitzer, A. 2014b. "TEST 14M - RCK02
560 : Part 1 - 9m radius centrifuge experiment on clayey levee behavior under ground motions",
561 Network for Earthquake Engineering Simulation (distributor),
562 Dataset, DOI:10.4231/D3W37KW7Z

563 Cappa, R., Brandenberg, S.J. and Lemnitzer, A. 2017. "Strains and pore pressures generated during
564 cyclic loading of embankments on organic soil." *Journal of Geotechnical and Geoenviromental*
565 *Engineering*, ASCE 143 (9). https://doi.org/10.1061/(ASCE)GT.1943-5606.0001721

566 Den Haan, E.J. 1996. "A compression model for non-brittle soft clays and peat."
567 Géotechnique 1996 46:1, 1-16, https://doi.org/10.1680/geot.1996.46.1.1

568 Deverel, A.J., Bachand, S., Brandenverg S.J., Jones C.E., Stewart, J.P., Zimmaro, P. 2016 "Factors
569 and proceesses affecting Delta levee system vulnerability". *San Francisco Estuary and*
570 *Watershed Science*, 14(4), Article 3

571 Dhowiana,. W., and Edil,T . B., 1980. "Consolidation behaviour of peats." *Geotechnical Testing*
572 *Journal*, 3(3), pp. 105-1 14.

573 Egawa, T., Nishimoto, S. and Tomisawa, K. 2004 "An Experimental Study on the Seismic
574 Behavior of Embankments on Peaty Soft Ground Through Centrifuge Model Tests", *13th World*
575 *Conference on Earthquake Engineering*, Paper No. 36.

576 Gray, H. 1936. "Progress report on the consolidation of fine-grained soils." *Proceedings of the*
577 *First International Conference on Soil Mechanics and Foundation Engineering.* Vol. 2,
578 Harvard University, Cambridge, 1936, pp. 138-141.

579 Kishida, T., Boulanger, R., Abrahamson, N., Driller, M.,Wehling, T. 2009 "Seismic Response of
580 Levees in the Sacramento-San Joaquin Delta." *Earthquake Spectra*. 25. 10.1193/1.3157259.

581 Kogure,K., Yamaguchi,H., Ohira,Y. and Ono,H. l986 "Experiments on Consolidation
582 Characteristics of a Fibrous Peat." *Proc. of Advances in Peatlands Engineering*,NRCC, 101-
583 108.

584 Kramer, S.L. 2000. "Dynamic Response of Mercer Slough Peat" *Journal of Geotechnical and*
585 *Geoenviromental Engineering*, ASCE, 126(6): 504-510.

586 Kutter, B. and Sathialingam, N. 1992. "Elastic-viscoplastic modelling of the rate-dependent
587 behaviour of clays" Géotechnique 1992 42:3, 427-441,
588 https://doi.org/10.1680/geot.1992.42.3.427

589 Lefebvre,G. et al. 1984 “Laboratory Testing and In-Site Behavior of Peat as Embankment
590 Foundation.” *Canadian Geotechnical Jour*., 21, 322-337.

591 Lemnitzer, A., Cappa, R., Yniesta, S. and Brandenberg, S.J. 2015 “Centrifuge Testing of Model
592 Levees atop Peaty Soil: Experimental Data”, *Earthquake Spectra*,
593 http://dx.doi.org/10.1193/032715EQS048

594 Lemnitzer, A. Brandenberg, S. Yniesta, S. Cappa, R. 2020 "TEST 16 - RCK16 : 1m radius
595 centrifuge experiment on clayey levee behavior under ground motions", in *NEES-2012-1161:*
596 *Levees and Earthquakes: Averting an Impending Disaster - Experiment 16*. DesignSafe-
597 CI. https://doi.org/10.17603/ds2-68kx-qm64.

598 Long M, Boylan N 2013 “Predictions of settlement in peat soils.” *Q J Eng Geol Hydrogeol*
599 46(3):303–322. doi:10.1144/qjegh2011-063

600 Lui, K., Xue, J., and Yang, M. 2016. “Deformation behaviour of geotechnical materials with gas
601 bubbles and time dependent compressible organic matter.” *Engineering Geology*, 213 (2016),
602 98-106

603 MacFarlane, I. C. and Radforth, N. W., "A Study of the Physical Behavior of Peat Derivatives
604 Under Compression," in *Proceedings of the Tenth Muskeg Research Conference*, National
605 Research Council of Canada, University of Toronto Press, Montreal, Canada, 1965

606 Mesri, G., Stark, T.D., Ajlouni, M.A. and Chen, C.S. 1997. “Secondary Compression of Peat with
607 or without Surcharging”, *Journal of Geotechnical and Geoenvironmental Engineering*, ASCE,
608 123(5): 411-421.

609 Meyer, Z., Coufal, R., Kowalow, M., Szczygielski, T., 2011 “Peat Consolidation – New
610 Approach”. Archives of Civil Engineering, LVII, 2, DOI: 10.2478/v.10169-011-0013-5

611 Shafiee, A., Stewart, J.P., and Brandenberg, S.J. 2015. “Reset of secondary compression clock for
612 peat by cyclic straining”, *Journal of Geotechnical and Geoenvironmental Engineering*, ASCE,
613 141(3).

614 Shafiee, A. 2016. “Cyclic and post-cyclic behavior of Sherman Island Peat”, *PhD Dissertation*,
615 University of California, Los Angeles.

616 Stokoe, K. H., Bay, J.A., Rosenblad, B.L., Huang, S. & Twede, M. 1994 “In situ seismic and
617 dynamic laboratory measurements of geotechnical materials at Queensboro bridge and
618 Roosevelt island.” Geotechnical Engrg. Rep. GR 94-5, Civ. Engrg. Dept., University of Texas
619 at Austin, Tex. 1994.

620 Taylor, D. W. & Merchant, W. 1940 ”A theory of clay consolidation accounting for secondary
621 compressions.” *J. Math. Phys.* 19, 167.

Terzaghi, K. 1923 “Die Berechnung der Durchlässigkeitsziffer des Tones aus dem Verlauf der hydrodynamischen Spannungserscheinungen.“ (In German.) Sitz. Akad. Wissen. Wien, Math-Naturw. Kl. Abt. IIa. 132:105–124.

Terzaghi, K., Peck, R.B., and Mesri, G. 1996. “Soil Mechanics in Engineering Practice“, 3rd Ed., Wiley, New York, NY.

Tokimatsu, K. and Sekiguchi, T. 2007. “Effects of Dynamic Properties of Peat on Strong Ground Motions During 2004 Mid Niigata Prefecture Earthquake”, *4th International Conference on Earthquake Geotechnical Engineering*, Paper No. 1531.

Wehling, T.M., R.W. Boulanger, R. Arulnathan, L.F. Harder and M.W. Driller 2003 “Nonlinear dynamic properties of a fibrous organic soil”, *Journal of Geotechnical and Geoenvironmental Engineering*, ASCE, 129(10): 929-939.

Wilson, . E., and Lo, M. B. 1965. “The progress of consolidation in an organic soil.” *Proceedings, Eleventh Muskeg Research Conference*, National Research Council, Technical Memorandum 87, pp. 1- 12.

Zhang, L. and O’Kelly, B. 2013 “The principle of effective stress and triaxial compression testing of peat.” *Proceedings of the Institute of Civil Engineers,* Vol 167, Issue GE1, pp. 40-50, https://doi.org/10.1680/geng.12.00038

639 **Table 1: Model parameters for the large scale and small-scale experiments. Dimensions in prototype scale.**

Experiment	Centrifugal Acceleration (g)	Levee crest width (m)	Levee base width (m)	Levee height (m)	Levee side slope (H:V)	Peat layer thickness (m)	Sand layer thickness (m)
Exp 12	57	10.3	30.8	5.1	2:1	9.4	3.4
Exp 14	57	10.3	30.8	5.1	2:1	6.1	8.6
Exp 16	50	5.0	10	2.0	5:4	2.6	1.0

640

641

642

643 **Table 2: Motions investigated for Exp 12, 14 and 16**

Experiment	Motion	Unscaled Magnitude M_w	Record/ Component	Peak Base Acc. [g] *prototype*	Scale Factors
Exp 12	Medium Loma Prieta	6.9	LGPC090	0.21	0.3
Exp 12	Large Kobe	6.9	Kobe0807	0.54	5.1
Exp 12	Large Loma Prieta	6.9	LGPC090	0.45	1.0
Exp 14	Sine Sweep 1	-	SWP7_333	0.02	0.1
Exp 14	Large Kobe	6.9	Kobe0807	0.53	5.1
Exp 14	Large Loma Prieta	6.9	LGPC090	0.42	1.0
Exp 16	2010 Maule EQ	8.8	CCSP_E	0.95	2.5
Exp 16	Sine Sweep	-	Sweep	0.85	0.6

644

645

646 **Table 3: Material Properties of Peat, Monterey Sand, and Modeling Clay**

Material Properties	***Peat***	***Monterey Sand***	***Modeling Clay***
average organic content, OC [%]	69	-	-
total unit weight, γ_t, [kN/m^3]	10.3 - 11.0	20.2	18
specific gravity of solids, G_s	1.79	2.64	-
initial void ratio, e_0	12 - 15.5	-	-
ave. compression index (Oedometer), *Cc*	3.9	-	-
shear wave velocity $V_s = V_{s1}(\sigma_v')^n$ [m/s]	Vs_1 = 54.2 m/s n = 0.16	Vs_1 = 195 m/s n = 0.26	Vs_1 = 400 m/s n = 0
P-wave velocity [m/s] @ 1g	400		-
relative density D_R [%]	-	90	
hydraulic conductivity, k [m/s]	-	10^{-4}	

647

648

649 **Table 4: Model input parameters for settlement simulation**

Property	Symbol	Value
Compressibility properties		
Virgin compression index	C_c	3.9
Recompression index	C_r	0.4
Reference pressure	$\sigma'_{v,ref}$	100 kPa
Reference void ratio	$e_{\sigma v',ref}$	5.4
Specific gravity of solids	G_S	1.85
Permeability properties		
Reference permeability	k_{ref}	2.0×10^{-7} m/s
Reference void ratio	$e_{k,ref}$	6.3
Coefficient of permeability variation	C_k	1.5
Secondary compression properties		
Secondary compression index	C_α	0.195
Reference time	t_{ref}	235.7 s
Reference void ratio	$e_{c\alpha,ref}$	5.4 (if $I_R = 0$)
Reference vertical effective stress	$\sigma'_{c\alpha,ref}$	100 kPa

650

Figure captions

Figure 1: Traditional time-based consolidation framework depicting the variation of *e* with log *t* under a given load increment

Figure 2: Generalized test layout for experiments Exp 12, 14, and 16

Figure 3: Slow data for (a) Exp 12, (b) Exp 14, and (c) Exp 16 depicting centrifuge accelerations (top), pore pressure time histories (middle) and settlement time histories (bottom)

Figure 4: Fast data sample for (a) Exp 14 Large Kobe motion, and (b) Exp 16 Maule, Chile EQ motion; acceleration (top), pore pressures (middle) and co-seismic settlements (bottom); time in prototype scale

Figure 5: Sample detail showing pore pressures and settlements during and after seismic loading

Figure 6: Example of equivalent direct simple shear time history for the location of sensor P7 during the Large Kobe motion in Exp 14.

Figure 7: Settlement and reset mechanism in terms of consolidation behavior (a), settlement-time history (b), and pore pressure dissipation vs. time (c) during the centrifuge experiment

Figure 8: Calibration of settlement rate using spin-up data from centrifuge test RCK01

Figure 9: Comparison of experimental and numerical settlements

Figure 10: Comparison of measured and predicted settlements at end of secondary compression with error analysis

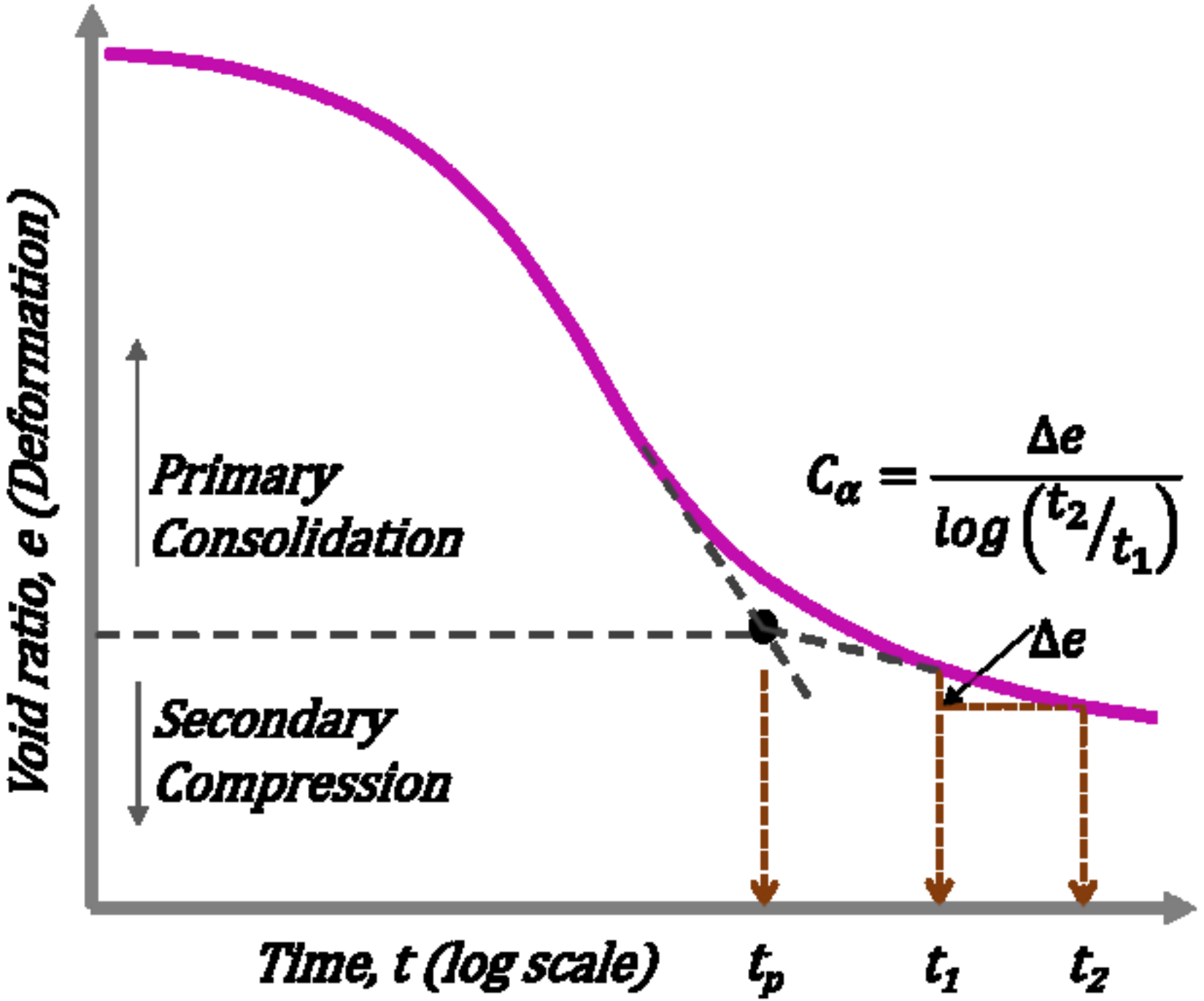
Void ratio, e (Deformation)
Primary Consolidation
Secondary Compression
$C_\alpha = \frac{\Delta e}{\log\left(t_2/t_1\right)}$
Δe
Time, t (log scale)
t_p
t_1
t_2

Fig 1

Fig 2

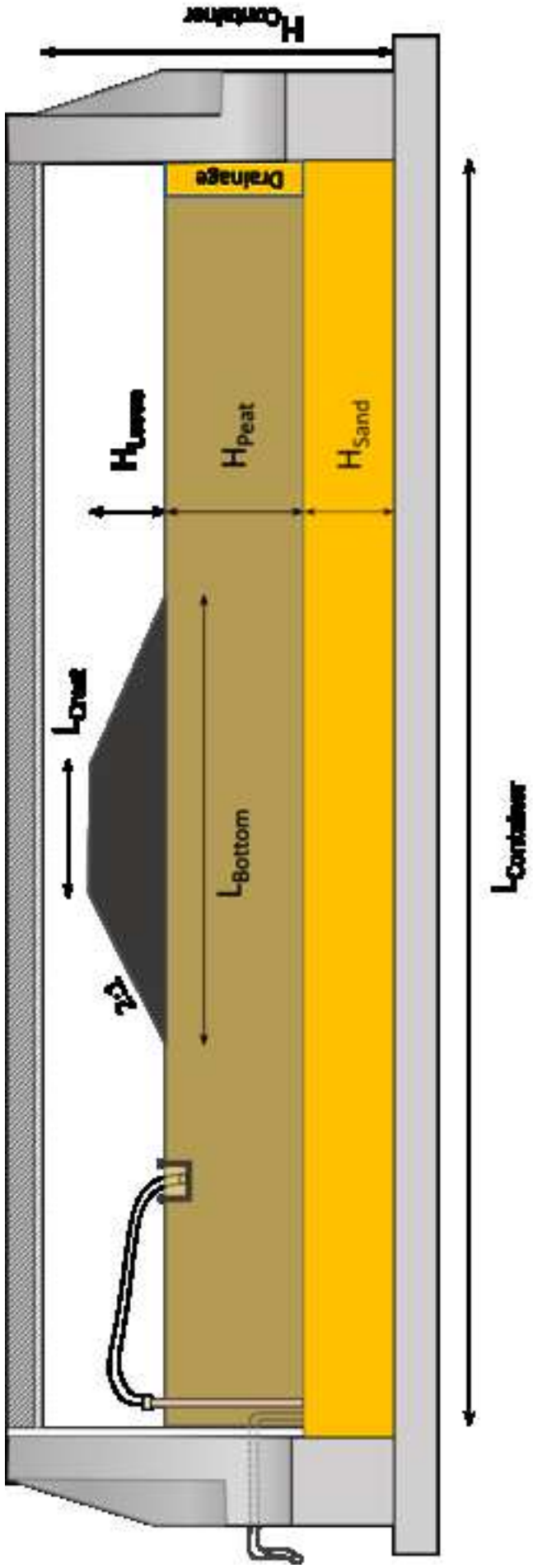
H_Container
Drainage
H_Unsat
H_Peat
H_Sand
L_Crest
L_Bottom
L_Container

Fig 3

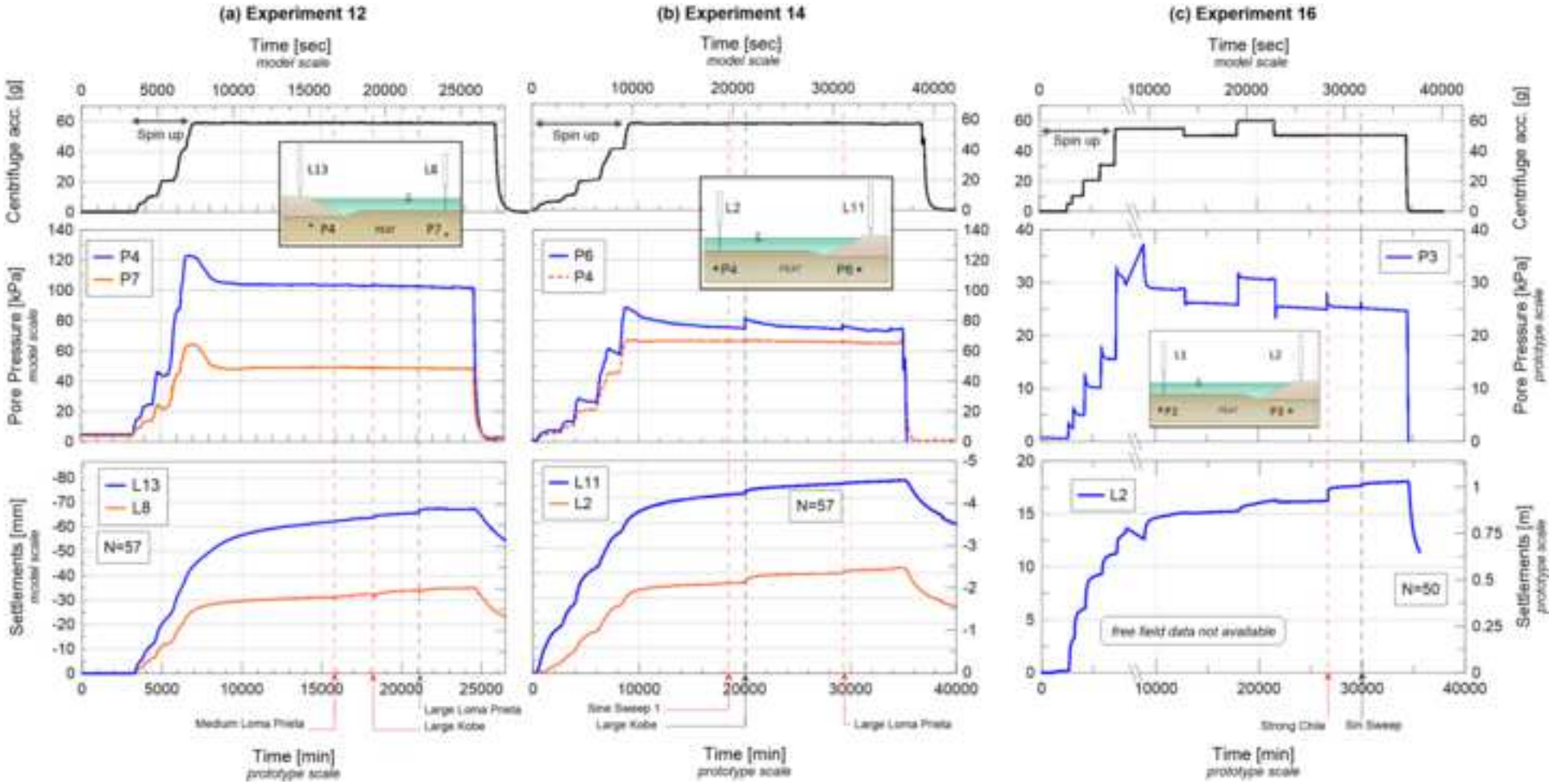
(a) Experiment 12
(b) Experiment 14
(c) Experiment 16
Time [sec]
model scale
Centrifuge acc. [g]
Spin up
Pore Pressure [kPa]
model scale
prototype scale
P4
P7
P6
P3
Settlements [mm]
Settlements [m]
L13
L8
L11
L2
N=57
N=50
free field data not available
Medium Loma Prieta
Large Loma Prieta
Large Kobe
Sine Sweep 1
Strong Chile
Sin Sweep
Time [min]
prototype scale

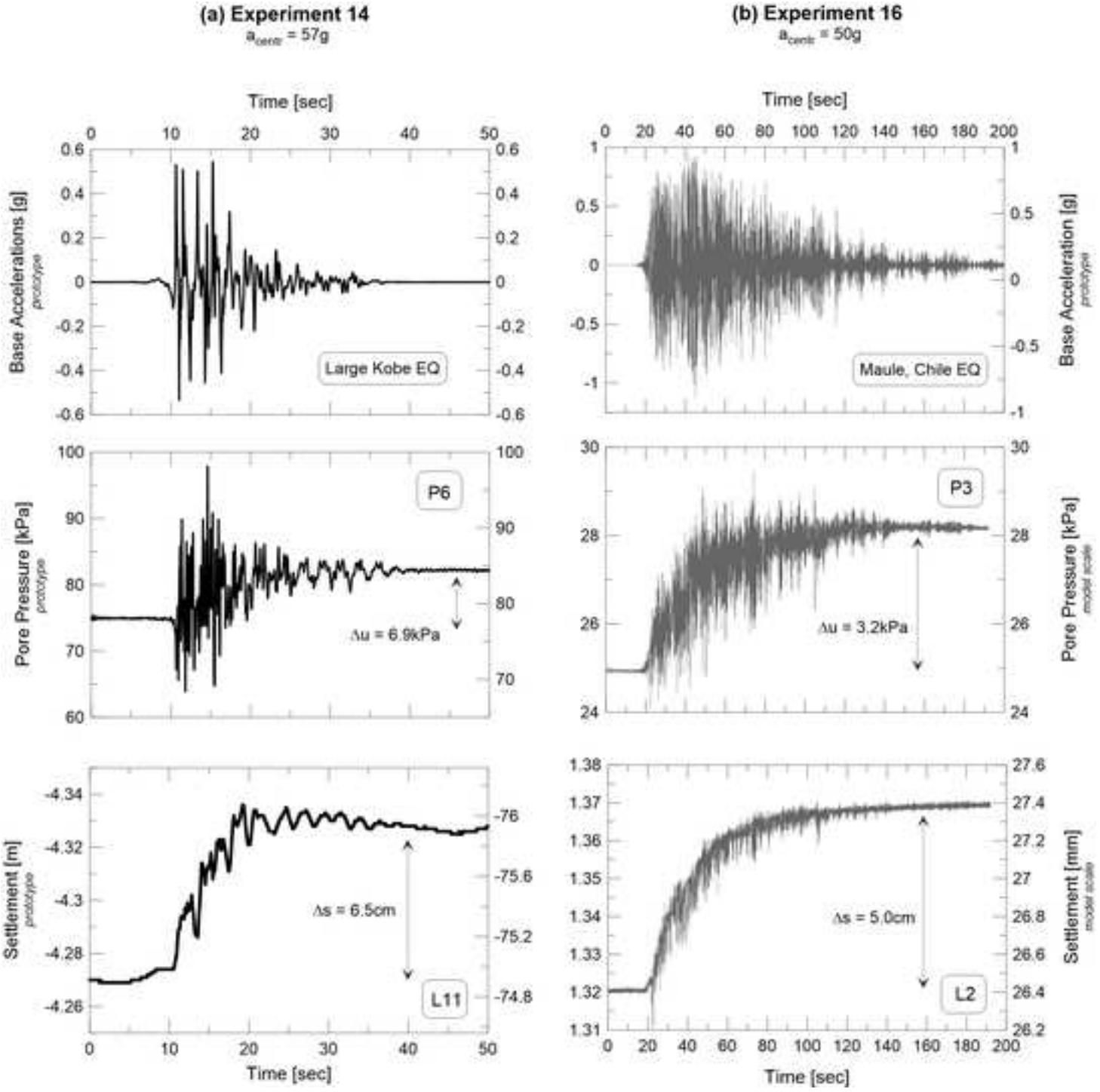
(a) Experiment 14
a_{cent} = 57g
(b) Experiment 16
a_{cent} = 50g
Time [sec]
Base Accelerations [g]
prototype
Large Kobe EQ
Maule, Chile EQ
Base Acceleration [g]
Pore Pressure [kPa]
prototype
P6
P3
Δu = 6.9kPa
Δu = 3.2kPa
Pore Pressure [kPa]
model scale
Settlement [m]
prototype
Δs = 6.5cm
Δs = 5.0cm
L11
L2
Settlement [mm]
model scale

Fig 5

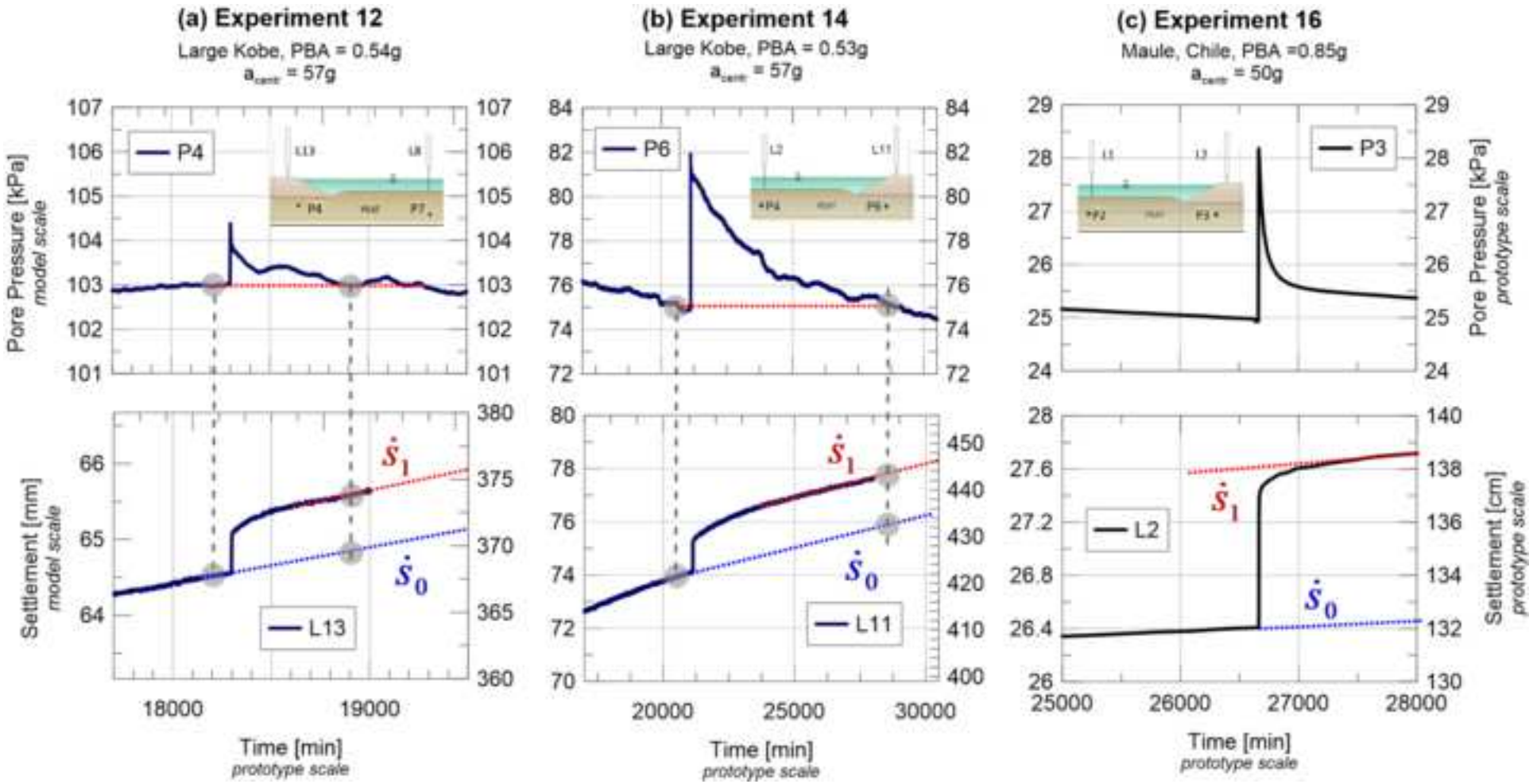
(a) Experiment 12
Large Kobe, PBA = 0.54g
a_centr = 57g
(b) Experiment 14
Large Kobe, PBA = 0.53g
a_centr = 57g
(c) Experiment 16
Maule, Chile, PBA =0.85g
a_centr = 50g
Pore Pressure [kPa]
model scale
prototype scale
Settlement [mm]
model scale
Settlement [cm]
prototype scale
P4
P6
P3
L13
L11
L2
$\dot{s}_1$
$\dot{s}_0$
Time [min]
prototype scale

Fig 6

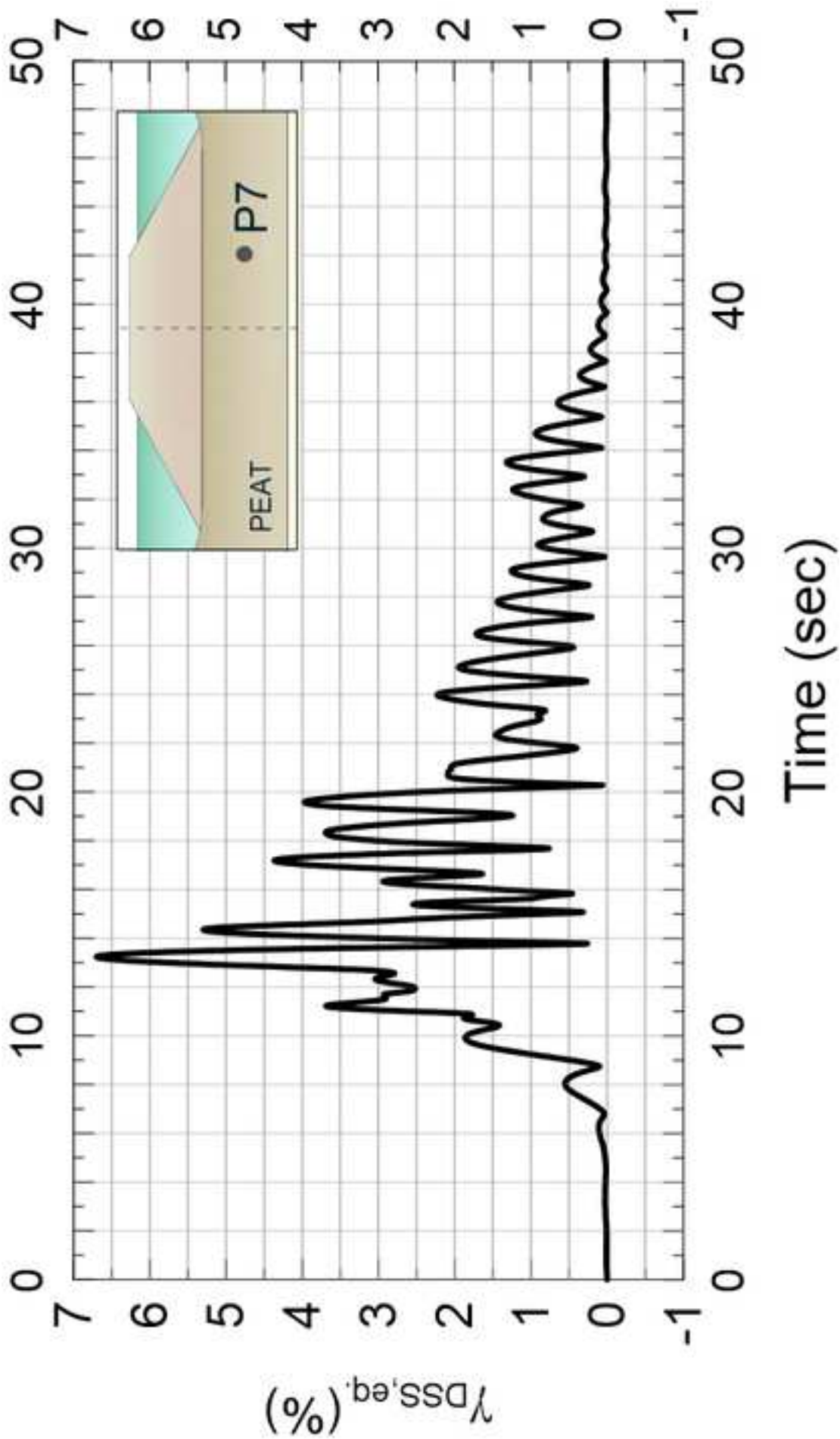

Fig 7

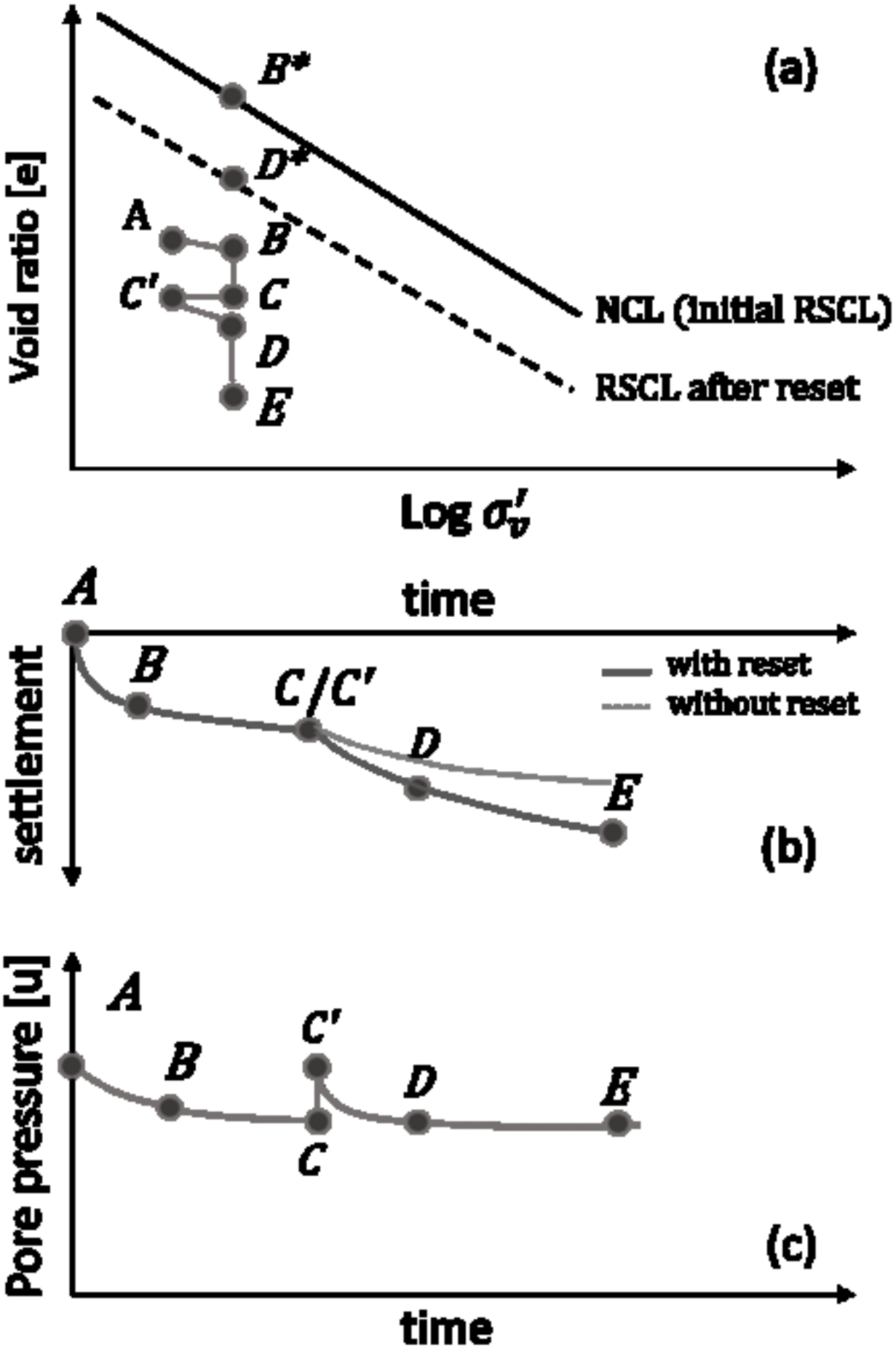
B*
(a)
D*
A
B
C'
C
D
E
Void ratio [e]
NCL (Initial RSCL)
RSCL after reset
Log σ'_v
A
time
B
C/C'
with reset
without reset
D
E
settlement
(b)
A
C'
B
D
E
C
Pore pressure [u]
(c)
time

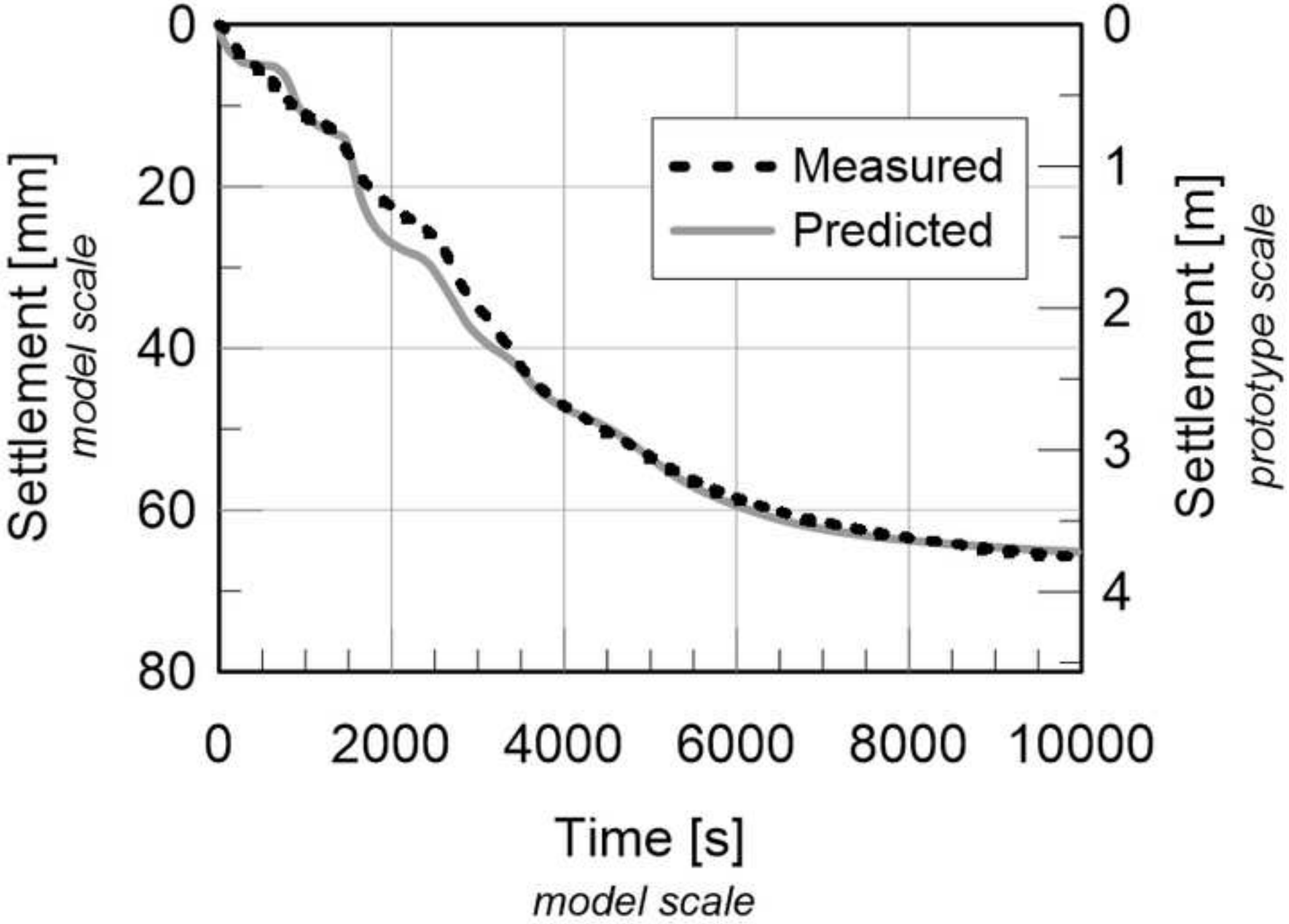
Settlement [mm]
model scale
0
20
40
60
80
Measured
Predicted
Settlement [m]
prototype scale
0
1
2
3
4
0
2000
4000
6000
8000
10000
Time [s]
model scale

Fig 8

Fig 9

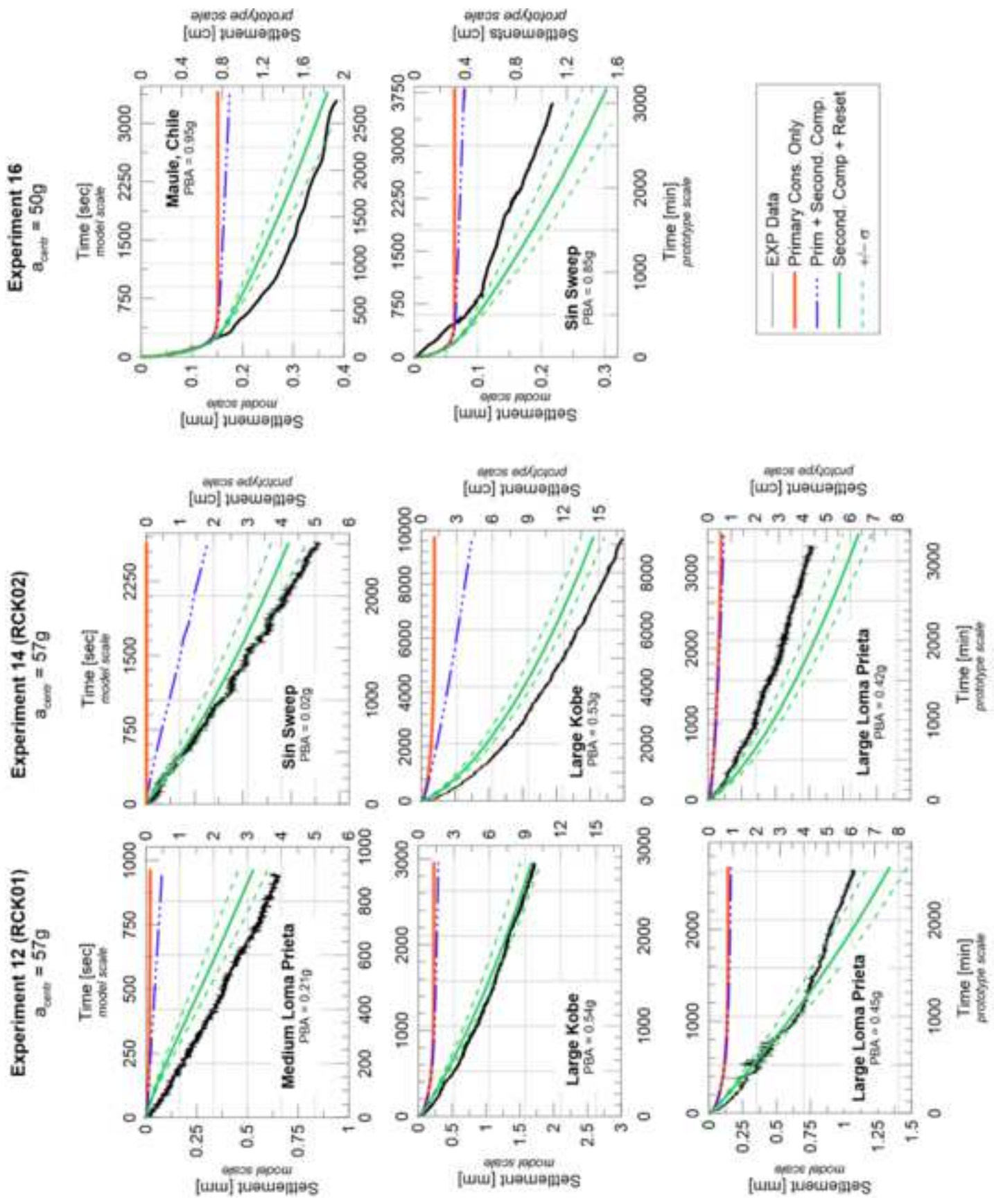
Experiment 12 (RCK01)
a_{centr} = 57g
Experiment 14 (RCK02)
a_{centr} = 57g
Experiment 16
a_{centr} = 50g
Time [sec]
model scale
Time [min]
prototype scale
Settlement [mm]
model scale
Settlement [cm]
prototype scale
Medium Loma Prieta
PBA = 0.21g
Large Kobe
PBA = 0.54g
Large Loma Prieta
PBA = 0.45g
Sin Sweep
PBA = 0.02g
Large Kobe
PBA = 0.53g
Large Loma Prieta
PBA = 0.42g
Maule, Chile
PBA = 0.95g
Sin Sweep
PBA = 0.85g
EXP Data
Primary Cons. Only
Prim + Second. Comp.
Second. Comp + Reset
+/- σ

Fig 10

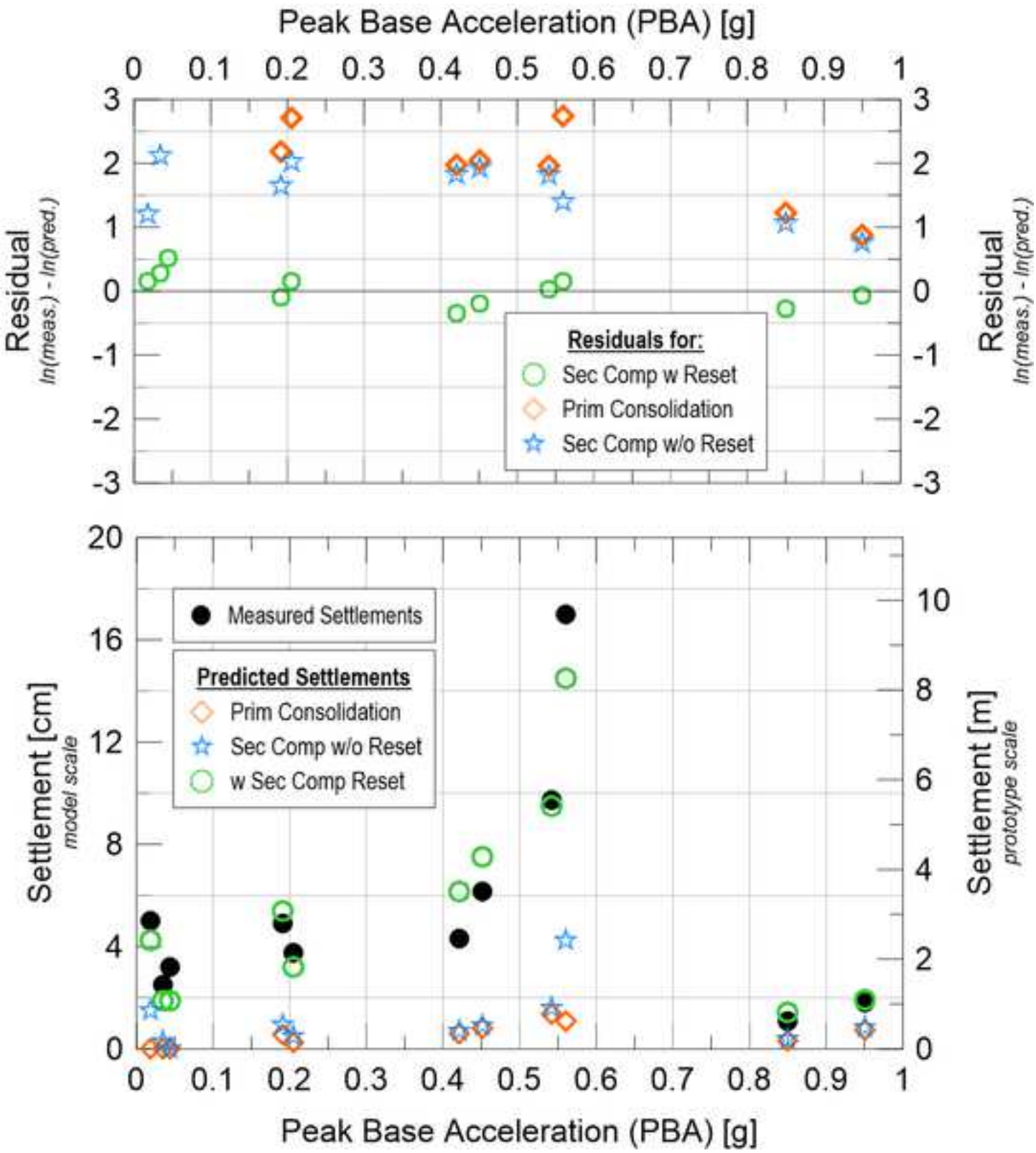
Peak Base Acceleration (PBA) [g]
Residual
ln(meas.) - ln(pred.)
Residuals for:
Sec Comp w Reset
Prim Consolidation
Sec Comp w/o Reset
Measured Settlements
Predicted Settlements
Prim Consolidation
Sec Comp w/o Reset
w Sec Comp Reset
Settlement [cm]
model scale
Settlement [m]
prototype scale
Peak Base Acceleration (PBA) [g]